Optically detected magnetic resonance to characterize atomlike microwave-optical transducers

Li Ma, Luke S. Trainor, Gavin G. G. King, Harald G. L. Schwefel, and Jevon J. Longdell*
Department of Physics, University of Otago, Dunedin 9016, New Zealand
and The Dodd-Walls Centre for Photonic and Quantum Technologies, Dunedin 9016, New Zealand

(Received 3 November 2022; accepted 28 April 2023; published 15 May 2023)

We introduce a method for optically detected magnetic resonance for atomlike systems in an optical resonator. Driving the spin transitions of these systems with microwaves causes changes to the populations of the ground-state spin levels, which we detect by changes in the optical cavity frequency. The technique is useful for characterizing experiments aimed at quantum microwave-to-optical transduction because it provides a way of only probing the spin transitions of the atomlike systems that are in the optical resonator's mode. We demonstrate the technique using a cryogenic erbium-doped whispering-gallery-mode resonator inside a microwave resonator. We compare our results with more standard electron paramagnetic resonance to show that our optical modes are confined to a region of large microwave magnetic-field amplitude. Our optical modes have a Q factor better than 10^8 making them the highest Q-factor resonators studied with cryogenic rare-earth-ion dopants, allowing us to report ensemble strong coupling between the erbium dopants and an optical whispering-gallery-mode resonator.

DOI: 10.1103/PhysRevA.107.053514

I. INTRODUCTION

Superconducting qubits operate at frequencies of about 10 GHz and hence must be kept at temperatures of tens of millikelvins in order to not be swamped by thermal photons, leading to a loss of fidelity. Interconnecting qubits in different cryostats is therefore difficult as a direct link would need to operate at a similar temperature [1]. The suggested alternative is coherently transducing the microwave photons to optical frequencies where they can propagate through room-temperature links with minimal thermal background [2,3].

Rare-earth ions in solids at cryogenic temperatures are great contenders for efficient microwave-optical transduction due to a unique set of capabilities for coherently manipulating information. The $4f - 4f$ transitions have very narrow homogeneous [4–6] and inhomogeneous [7,8] optical linewidths, as well as long-lived coherence times for both nuclear- [9] and electron-spin transitions [10,11]. Although the ions typically have weak optical oscillator strengths, this can be compensated by the narrow linewidths to give high optical absorption, even to the point where negative refractive index could be possible [12]. The use of erbium dopants, in particular, gives access to an optical transition at 1.5 μm, in the center of the low-loss wavelength region for optical fibers.

These properties of rare-earth-ion dopants have enabled a number of advances in quantum memories [9,13] and classical signal processing [14,15]. A particular advantage of using dopants over free space atoms is increased flexibility when coupling the dopants to optical resonators. The coupling of rare-earth-ion dopants to nanophotonic resonators has enabled single-site detection [16] as well as control and readout of single dopants [17]. Meanwhile, the coupling of ensembles to macroscopic resonators has been investigated to improve quantum memories [18] and microwave-optical transduction [19–21].

The ions' optical and spin transitions provide a nonlinearity for frequency conversion. For efficient transduction, generally both microwave and optical resonators are used to increase the coupling between the input and output fields with the nonlinear system used for the frequency conversion. A major challenge of such a nonlinear converter is that the vastly different optical and microwave wavelengths make obtaining a good spatial overlap difficult. Here we introduce a method for optically detected magnetic resonance (ODMR), for atomlike systems in an optical cavity, which provides a way to only probe ions at the intersection of the microwave and optical resonator modes. The method is a useful experimental check of overlap, particularly as microwave modes can be very sensitive to perturbations such as unintentional gaps between components.

ODMR is a powerful technique for probing solid-state spins. Standard ODMR works by looking at spin-state-dependent changes in the amount of optical absorption or fluorescence level, as either property depends on the population balance [22,23]. ODMR is a more sensitive technique than direct electron-paramagnetic-resonance (EPR) spectroscopy, not only due to the higher-energy probe photons, but also because thermal noise is much lower at optical frequencies. The optical detection significantly improves the sensitivity of magnetic-resonance spectroscopy and increases the fidelity and spatial resolution of spin initialization and readout [24–26].

In our system we perform ODMR by monitoring changes in the material's dispersion rather than absorption. We demonstrate the technique using a high-quality-factor erbium-doped whispering-gallery-mode (WGM) resonator made from yttrium orthosilicate (Y_2SiO_5, YSO). This dispersive

*jevon.longdell@otago.ac.nz

measurement is enhanced by strong coupling between an optical resonator mode and an ensemble mode of the rare-earth ions. In this strong-coupling regime, the WGMs hybridize with the erbium ensemble, such that they are polaritons. Through the change of this WGM-ensemble polariton's frequency we measure the change in coupling due to exciting more ions into the upper spin state.

Whispering gallery mode resonators combine extremely high Q factors and moderately small mode volumes in a convenient monolithic form factor [27]. The guiding of light is provided by total internal reflection from the curved surface of the resonator's rim. Thus the resonators can operate over a wide range of wavelengths and can be made of any optical material that is low loss and for which smooth surfaces can be prepared. For example, recently Q factors of 10^9 have been demonstrated [28] for yttrium orthosilicate (YSO)—a popular host for cryogenic rare-earth-ion dopants because of its low density of spins.

The flexibility in material choice for WGM resonators has allowed numerous nonlinear optical processes like second-harmonic generation [29–31], Kerr solitons [32,33], and optical parametric oscillation [34] in wide frequency ranges. The high Q factors have enabled efficient demonstrations of photon pair sources [35] and allowed squeezing measurements of optical parametric oscillation operated far above threshold [36]. Interfacing a microwave field with the resonators has allowed for electro-optic demonstrations such as efficient single-sideband modulation [37] and electro-optic frequency combs [38,39]. Coupling to ensemble spin states has previously been achieved through the interaction with magnon modes of yttrium iron garnet spheres [40].

Studies of doped WGM resonators have shown their flexibility as lasers [41–43]. Cryogenic rare earths in WGM resonators, however, are relatively unexplored, in spite of the promises of high Q factors for both the resonators and the ions. It has been shown that being near to the surface in a WGM resonator does not adversely affect the ions' spectral properties [44].

Our WGM resonator fulfils the promise of high Q factors and shows strong coupling to an optical transition in erbium. The ODMR measurement we introduce allows us to characterize the microwave-optical overlap. The technique can be applied to other atomlike transduction schemes.

II. EXPERIMENTAL SETUP

Our WGM resonator is made from YSO doped with isotopically enriched erbium-170 at 50 ppm. The resonator is a disk of major radius $R = 2.1$ mm and thickness of 0.5 mm, with its curved sidewall surface finely polished by diamond slurry [45]. The crystal D_2 axis is normal to the disk plane. It is well known that YSO has yttrium ions sitting in two different crystallographic sites each with two different orientations [46]. Here we address the erbium ions at site 1 with the optical transition around $\nu_0 = 195116.7$ GHz—a wavelength of about 1536 nm in the telecom C band.

The optical pump couples into the WGM resonator by a right-isosceles gadolinium gallium garnet prism via evanescent coupling. Such a prism conveniently allows for coupling

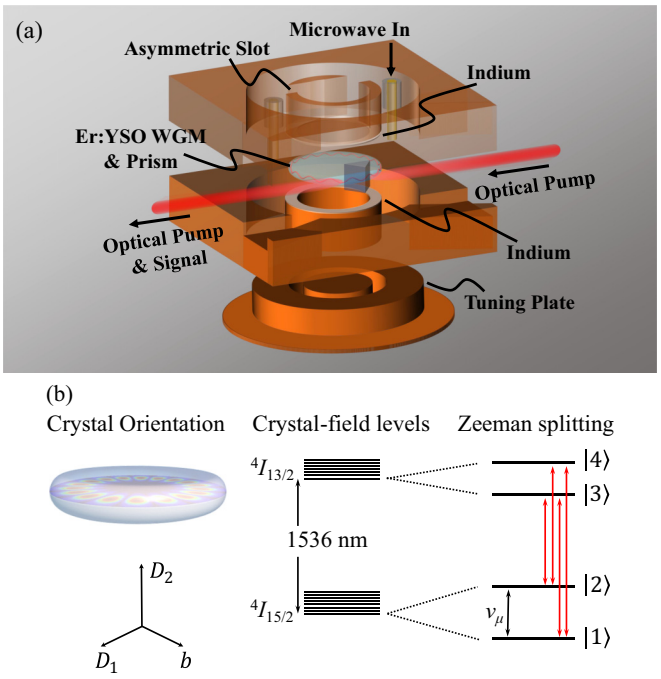

FIG. 1. (a) Schematic of the ODMR apparatus. The microwave resonator (orange) is a shielded copper cavity with the top and bottom rings that clamp onto the WGM resonator. Two coaxial pins (gold) are used for coupling microwave in and out of the cavity. The WGM resonator (light blue disk) is placed between the copper rings, with a prism (dark blue) that couples the optical pump (red) to the WGM resonator via evanescent coupling. (b) Crystal orientation and energy-level diagram of the erbium ions. With an external magnetic field, the crystal-field levels of $^4I_{15/2}$ and $^4I_{13/2}$ have split due to the Zeeman effect. ν_μ shows the microwave transition that interacts with our microwave resonator; also shown are the four optical transitions that interact with the optical resonator in ascending order of energy.

with a straight-through geometry in the cryostat. The crystal's b axis points from the disk center to the coupling prism. The prism is moved by a linear piezo stage to accurately tune the extrinsic optical coupling rate. We label WGMs with their electric field parallel to the D_2 axis as the transverse electric (TE) polarization; those polarized in plane are transverse magnetic (TM). TM modes have lower coupling contrast than TE modes due to their different local refractive indices at the coupling point.

The WGM resonator sits inside a microwave resonator—see Fig. 1(a)—which uses two metal rings, above and below the optical WGM resonator, to confine the microwave mode near the optical-mode volume. The resonator is based on previous designs [47]; one modification here is that to allow a greater tuning range, the whole floor of the resonator was movable rather than just a tuning pin. Another modification is that the top ring has an asymmetric slot, designed to break the near twofold rotational symmetry of the microwave magnetic field and relax the phase-matching requirements for future up-conversion experiments. A layer of indium is used between the metal rings and WGM resonator to reduce the gap between the two and better clamp the resonator.

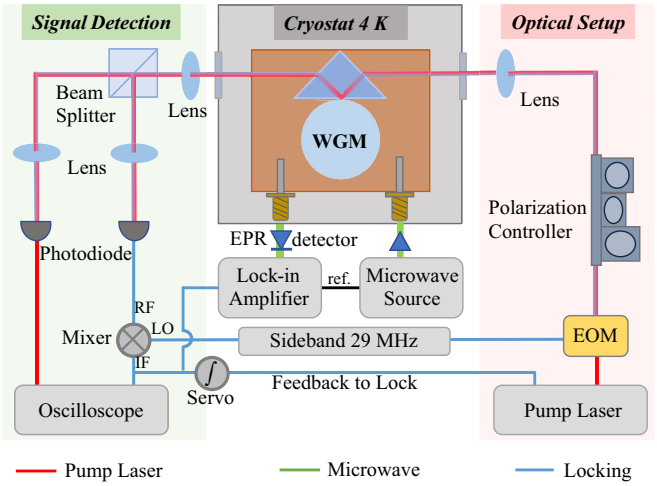

FIG. 2. Schematic of the experimental setup and measurement. A tunable laser of 1536 nm acts as an optical pump, with an EOM for relative frequency measurement and a polarization controller for WGM coupling. The microwave transition is driven by a microwave source with frequency around 12.155 GHz. The reflected light is collected and detected by two photodiodes for optical monitoring and locking. When EPR is measured, the microwave source is frequency modulated and the resulting amplitude changes on the microwave output are measured by a microwave power detector and lock-in amplifier. When ODMR is being measured the microwave source is amplitude modulated and the resulting optical-mode frequency oscillation is detected by a lock-in amplifier. The color lines in the bottom indicate the different frequencies of pump laser, microwave, and sideband modulation.

The crystal orientation was chosen to allow up-conversion with the in-plane microwave magnetic field provided by the microwave cavity [48,49].[1]

The combined optical and microwave resonators were mounted in a home-built cryostat. The base temperature is 4 K, which can be temporarily reduced to 2.9 K by a helium evaporation system. A three-dimensional (3D) vector magnet (300 mT along the main axis; 10 mT in each of the other two axes) applies a tunable external magnetic field along the D_2 axis. The magnetic field causes Zeeman splitting of the ${}^4I_{13/2}$ and ${}^4I_{15/2}$ transition which we examine here; see Fig. 1(b). The cryogenic environment substantially reduces phonon-based dephasing mechanisms which would otherwise broaden both the spin and optical transitions to many gigahertz.

The experimental setup is shown in Fig. 2. A tunable fiber laser around 1536 nm is focused by lenses outside the cryostat onto the prism-resonator interface for evanescent coupling and the reflected light is collected on a photodiode. An electro-optic phase modulator (EOM) and second photodiode are used for generation of a Pound-Drever-Hall (PDH) error signal. This error signal will be used for two purposes in the ODMR spectroscopy: it allows us to lock the laser to optical modes with a servo, as well as measure changes in the resonant frequencies that occur faster than the servo can react.

The EOM also allows for accurate relative frequency calibration for measuring optical linewidths and free spectral ranges (FSRs). At base temperature, we measured the intrinsic linewidth of a TE mode at 195 126.5(4) GHz—about 10 GHz away from the optical transition of Er^{3+}—to be 1.32(10) MHz, corresponding to a quality factor of $1.48(12) \times 10^8$. A TM mode about 0.9 GHz lower in frequency had a quality factor of $1.07(7) \times 10^8$. Meanwhile, the optical modes have a free spectral range (FSR) of around 12.3 GHz and the tunable range of the microwave resonance frequency is approximately 0.15 GHz centered around 12.15 GHz. By moving the microwave tuning plate in and out, we can choose the microwave resonance frequency and make it match the optical FSR. This frequency matching will be critical for future up-conversion experiments, as it means that all three modes—optical pump, optical signal, and microwave—can be resonant at the same time, enhancing the efficiency.

The coupling of optical modes to the erbium ions was measured by scanning the laser via its internal piezo and tuning the external magnetic field to linearly change the erbium ions' optical transitions. Figure 3(a) shows a 2D map of the optical spectrum with an applied magnetic field nearly along the resonator's D_2 axis. Each line is an optical mode with its corresponding anticrossings where it approaches degeneracy with the erbium transitions. The four straight dashed lines indicate the transitions between different energy levels.

To measure the coupling between the microwave resonator and the Er^{3+} spin transition, we use a frequency-modulation EPR technique [50,51], with a setup similar to our previous work [52]. The microwave source couples a frequency-modulated microwave tone into the cavity by the input coaxial pin mounted at the top of the microwave cavity. A microwave power detector rectifies the microwave output from an output pin and a lock-in amplifier detects the modulation thereon which gives an error signal; through the modulation and lock-in detection we accurately sense the *derivative* of the absorption profile. Measurement of the error signal at different microwave carrier frequencies provides us with a reference to convert between error signal level and microwave frequency detuning.

Next the microwave carrier frequency is fixed close to the cavity frequency. When the Zeeman splitting of the ground state approaches resonance with the microwave cavity, the cavity resonant frequency is pulled by the ions causing the error signal to shift, which we can convert into a frequency excursion, as shown in Fig. 3(b). As we expect the Er^{3+} spectral density to be a Gaussian distribution—mainly defined by the inhomogeneous broadening—we fit the response to the derivative of a Gaussian, from which we obtain measures of the inhomogeneous linewidth and the total peak-to-peak shift of the microwave resonant frequency.

[1]For example, up-conversion of a microwave photon with a TE optical pump to a TE optical signal is possible using χ_{yyz} in the C_{2h} section of Table I of Ref. [49]. In that table the z axis is the crystal's symmetry axis, so we can transform the conclusions into our coordinate axes by substituting $(x, y, z) \rightarrow (D_1, D_2, b)$. The TM case is also not reduced to zero by symmetry. We note that there will be additional nonlinear *permeability* components, as the optical transitions of Er^{3+} are magnetic-dipole active.

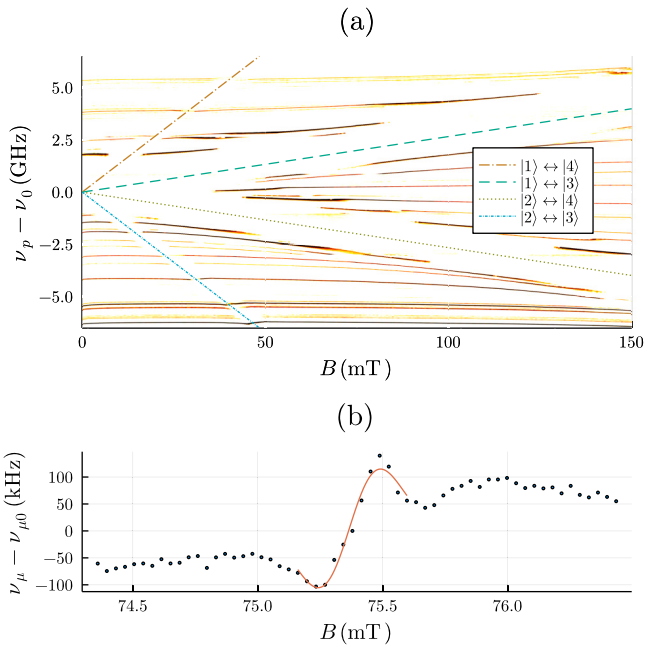

FIG. 3. (a) TE-polarized optical modes in the Er^{3+}:YSO resonator as a function of magnetic field. ν_0 is the zero-field ${}^4I_{15/2} \leftrightarrow {}^4I_{13/2}$ transition frequency. These modes are measured by the reflection from the coupling prism; dark lines show where light has coupled into the cavity. To increase visibility of the narrow modes on a large frequency scale, the reflection spectra are convolved with a 30 MHz wide top-hat function. Dashed lines show the optical transitions of the erbium ions, from which we can estimate the effective g factors of the ground and excited state are $g_{g,\mathrm{eff}} \approx 11.5$ and $g_{e,\mathrm{eff}} \approx 7.7$. These are about 10 % higher than the values measured along the D_2 axis by [46]. Some stitching errors can be seen, as a range of only ∼2.2 GHz was measured at a time. Slight increases in frequency of the modes near zero applied magnetic field are artifacts of the laser frequency settling over a long-time period. (b) EPR measurement of the microwave coupling via a shift in the microwave mode frequency. The fit is the derivative of a Gaussian distribution, from which we find the full width at half maximum of the transition, which is 47.4(3.5) MHz. From the EPR measurement we find $g_{g,\mathrm{eff}} = 11.52(25)$.

Prior to the EPR measurement shown, we first oriented the magnetic field with respect to the YSO crystal axes, as the resonator and magnetic-field coils will not be perfectly aligned. Site 1 of Er^{3+} in YSO has two distinct orientations related by C_2 symmetry [46]. By applying orthogonal magnetic fields B_y and B_x we could tune it such that the two orientations have equal effective g factors, as determined by EPR. This finds a nearby direction in the D_1–D_2 plane.

The measurement technique we introduce here is a variation on ODMR, possible due to the strong optical coupling between the WGMs and the collective erbium transitions. The PDH error signal is integrated by an open-software closed-hardware FPGA board [53], which feeds back into the laser's internal piezo to lock to the WGM. The microwave resonator is excited; if the driving frequency matches the Zeeman splitting of Er^{3+}, the populations of the spin states ($|1\rangle$ and $|2\rangle$) are brought closer together. The optical mode then shifts due to a change in coupling caused by this population change. The shift is seen by a change in the PDH error signal. The input microwave field is amplitude modulated with a modulation depth of 45 % and a modulation frequency of 1 kHz. The PDH error signal oscillates at this frequency as the erbium ions move between spin states. The lock-in amplifier detects amplitude modulation of the error signal at this frequency. Dual use of the error signal for both locking and detection is similar to the ac-magnetostrictive sensing performed in Ref. [54]. The lock-in amplifier signal is converted into a frequency shift based on the measured slope of the error signal around the optical resonant frequency. The servo applies a 151.8 Hz digital low-pass filter to its input to avoid the lock compensating for the modulation and thus reducing the signal measured by the lock-in amplifier. In contrast to regular ODMR where the population transfer is measured by changes to an absorption coefficient, we measure changes in coupling between our WGMs and an optical-frequency Er^{3+} transition.

We note that the ODMR introduced here can be understood as microwave and optical excitation and relaxation occurring one after another. This process has similar symmetry considerations to cross-phase modulation in nonlinear optics and is never reduced to zero by symmetry (unless of course either of the transition strengths is zero). Intuitively, as we change the erbium ions' spin state, there will be more (or less) absorption, which must result in a dispersion change due to the Kramers-Kronig relations.

III. RESULTS

Optically, we can measure the coupling to the erbium ions by observing the crossings. Figure 4(a) shows the avoided crossing of the erbium transition with two neighboring TM WGMs separated by about 80 MHz. The better coupled WGM has a frequency of $\nu_{p0} = 195\,112.8(4)$ GHz at zero applied magnetic field. This mode is chosen as it is one of the few TM modes that couples well. We can therefore assume it has a high effective refractive index and hence will have a low radial mode number ($q \approx 1$). Additionally, in the optical spectra one can very clearly see its anticrossing, especially around 140 mT, where both branches of the optical-erbium polariton are seen. A fit of the frequencies of both polariton branches—as determined by reflection minima—to an avoided crossing gives an ensemble coupling rate of $g_{\mathrm{ens,TM}} = 2\pi \times 0.85$ GHz, which can also be seen directly from the splitting of 1.7 GHz. The optical power is $P_p = 2.3$ mW and the maximum coupling efficiency to this mode is 10 %.

The input laser frequency is scanned in a sawtooth. Sweeping the frequency up gives a different line shape to sweeping in the opposite direction, which can be understood as a consequence of spectral hole burning. Say we are sweeping the laser frequency up as in the bottom halves of Figs. 4(a)–4(c). We first couple to the low-frequency branch of the optical-erbium polariton. Some of the erbium ions are excited into the optical excited state, which causes the optical-erbium coupling strength to decrease, and hence the low-frequency polariton increases in frequency. The polariton thus follows the pump laser somewhat, leading us to see a broadened line shape. For example, in Fig. 4(b) where a higher power of 15 mW is used, the bottom absorption line grows in width

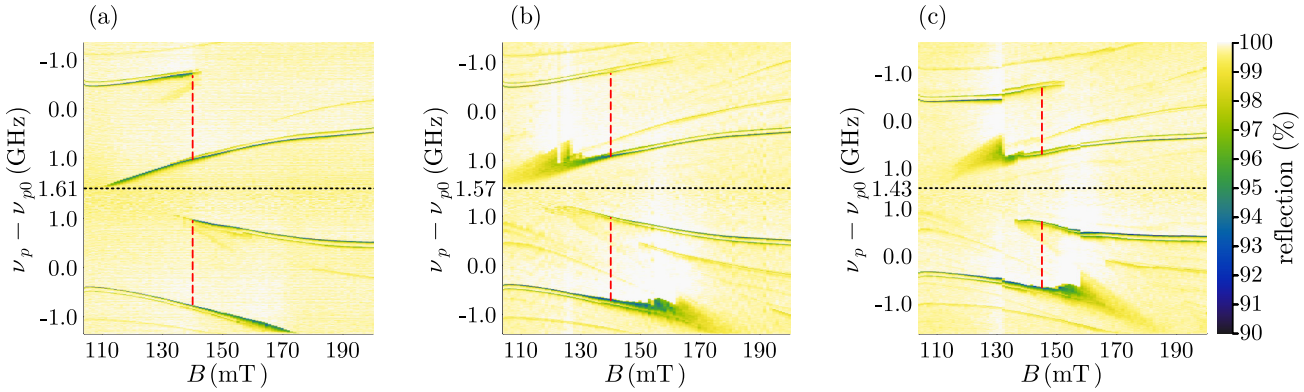

FIG. 4. Saturation of optical anticrossing with input optical power. The TM WGM has a zero-field frequency of $\nu_{p0} = 195\,112.8(4)$ GHz. The reflection of the optical resonator is measured over a range of about 3 GHz at different magnetic fields along the D_2 axis. At a field of 140 mT, one can see the mode splitting (red dashed lines) between the two branches of the resulting polariton. The frequency is swept by a triangle wave input to the lasers piezo from the bottom to the top of the graph. Both sides of the frequency sweep are shown to display the asymmetry caused by optical pumping. (a) $P_p = 2.3$ mW, $T \approx 4$ K; (b) $P_p = 15$ mW, $T \approx 4$ K; (c) $P_p = 15$ mW, $T \approx 2.9$ K.

with increasing magnetic field as the polariton becomes more erbiumlike and thus it tracks the increasing optical pump frequency more. When we increase the laser frequency and couple to the high-frequency polariton branch, hole burning causes the polariton to *decrease* in frequency; hence the line shape appears narrowed.

The optical powers reported are the geometric mean of the powers measured entering and exiting the cryostat when there is no coupling to the optical resonator, $P_p = \sqrt{P_{\text{enter}} P_{\text{exit}}}$. If all losses were due to Fresnel reflections, this would accurately give the power at the prism-resonator interface due to the symmetry of the optical path in the cryostat. However—as a small amount of clipping of the beam is observed—this power will be a slight overestimate.

A further change is seen by lowering the temperature of the cryostat. Figure 4 shows the same mode measured with 15 mW of input power with a lowered base temperature of about 2.8 K to 2.9 K as measured on the exterior of the microwave cavity before and after measurement. The jumps at about 132 mT and 158 mT show the significant decrease in optical pumping occurring between these two values.

The erbium ions strongly absorb in a narrow band near their transition frequency, which by the Kramers-Kronig relations results in strong localized dispersion. To gauge the dispersion induced by the erbium ions, we measure the FSRs of this TM mode family at zero applied magnetic field. This TM mode family is used because we have a low coupling contrast to other nearby TM modes. We can therefore rapidly identify modes across multiple FSRs, even when the modes have been shifted significantly by coupling to the erbium ions. The measurements are performed by sideband spectroscopy [55]. The input laser is swept across the resonance and modulated by the EOM. When the modulated frequency is equal to the FSR, the absorption dips from the carrier coupling to the probed resonance and a sideband coupling to the mode one FSR away coincide. By varying the modulation frequency and examining the transmitted line shapes the FSR can be measured to a resolution better than the linewidth. Seven consecutive FSR measurements are given in Table I. The group-velocity dispersion (GVD) β_2 can be approximated by

$$\beta_2 = \frac{\partial^2 \beta}{\partial \omega^2} = -\frac{1}{(2\pi)^2}\frac{\partial^2 \nu}{\partial \beta^2}\left(\frac{\partial \beta}{\partial \nu}\right)^3 \approx -\frac{1}{R(2\pi)^2}\frac{\nu_{m+1} - 2\nu_m + \nu_{m-1}}{(\nu_{m+1}/2 - \nu_{m-1}/2)^3}, \quad (1)$$

where $\beta = m/R$ is the propagation constant. The value of GVD with the largest magnitude is estimated to be $\beta_2 \approx -4.6 \times 10^9$ fs^{2}m^{-1}.

We characterize the microwave transition with EPR. Figure 3(b) shows a measured EPR response with a fit showing the peak-to-peak frequency shift of the microwave mode and Gaussian full width at half maximum (FWHM). Figure 5 shows the frequency shift at different powers, which decreases as the spin transition saturates. The microwave powers reported are the powers entering the cryostat; the power coupled into the microwave resonator is about 40 dB lower. Throughout these measurements the fitted FWHM stays relatively constant. We find a FWHM of 47.8 MHz, with an error of

TABLE I. Free spectral ranges (FSRs) of the TM mode family with a mode which has an azimuthal mode number of $m_{\text{ref}} \approx 15000$ and a frequency of $\nu_{m_{\text{ref}}} = 195\,112.8(4)$ GHz. This is the better coupled of the pair of modes shown in Fig. 4. The right column gives the difference between adjacent FSRs, which gives a measure of dispersion. All FSRs carry a measurement uncertainty of 0.5 MHz.

Mode number $m - m_{\text{ref}}$	FSR (GHz) $\nu_{m+1} - \nu_m$	ΔFSR (MHz) $\nu_{m+1} - 2\nu_m + \nu_{m-1}$
3	12.3255	13.0
2	12.3125	65.5
1	12.2470	-517.0
0	12.8180	731.0
-1	12.0870	-213.0
-2	12.3000	-21.5
-3	12.3215	

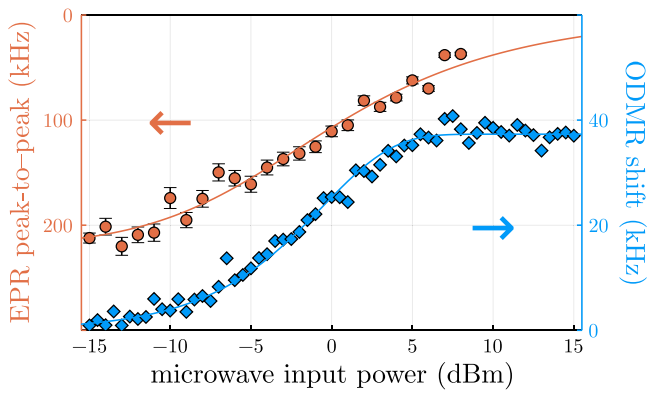

FIG. 5. Saturation of EPR and ODMR signals as the microwave power is increased. The EPR signal (orange circles, left axis) saturates towards zero at high microwave power because it is sensitive to the spin state population difference and at high microwave powers the spin states will have close to the same population. Only one of the two spin states is involved in the optical transition used for the ODMR. This means that the ODMR signal (blue diamonds, right axis) is predominantly sensitive to one of the two spin states and saturates to a nonzero value. The optical mode probed is a TE mode at 195 106.1(4) GHz, slightly lower in frequency than the one used for Fig. 6(a). The fitted saturation powers are −5.19(50) dBm for EPR and −0.54(15) dBm for ODMR. However, this is not a direct comparison as the fitting functions used are different, as mentioned in the text.

±0.7 MHz derived from the statistical uncertainty of the fits assuming they are independent, and an error of ±0.6 MHz from our systematic uncertainty in the magnetic-field hysteresis, which is common to all measurements carried out during the same magnet cooldown.

Next we examine the ODMR frequency shifts. We look at two sets of TE optical modes in different polariton regimes. TE modes are used for the ODMR measurements because our optical coupling achieves a better coupling contrast to them and there are more modes we couple to per FSR. Figure 6(a) shows the first pair of modes with a frequency of $\nu_{p0} = 195\,106.2(4)$ GHz. At a magnetic field of about 81 mT they cross the $|2\rangle \leftrightarrow |3\rangle$ transition. Figure 6(d) shows the second group of three modes with a frequency of $\nu_{p0} = 195\,112.7(4)$ GHz. Between about 100 mT and 200 mT they avoid the $|1\rangle \leftrightarrow |3\rangle$ transition. The fitted coupling rate is $g_{\mathrm{ens,TE}} = 2\pi \times 1.2$ GHz, also seen from the red dashed line showing that the frequency difference of the polariton branches is 2.4 GHz. Red stars on the top and bottom are located just beside the modes of interest. For clarity the color map is throttled at 90 %; the maximum coupling obtained for this mode is about 25 %. To simplify the error signal and to allow it to measure larger frequency shifts, we overcouple to these modes in later experiments such that the error signal is monotonic around the resonance frequency.

The volume of a fundamental WGM in our cavity is about $V = 1.5 \times 10^{-12}$ m^3 [56,57]. In this volume there will be about $N_2 = 3.1 \times 10^{11}$ site-1 erbium ions in the upper Zeeman state $|2\rangle$ at a field of 140 mT. The single-ion coupling rate is then $g_c = g_{\mathrm{ens}}/\sqrt{N_2}$, which is $2\pi \times 1.5$ kHz for the TM mode in Fig. 4, which corresponds to a transition dipole moment of

$$\mu = n_p g_c \sqrt{\frac{2\hbar\epsilon_0 V}{2\pi\,\nu_p}} = 2.6 \times 10^{-32}\,\mathrm{Cm}, \tag{2}$$

where n_p is the refractive index. This is similar to other values in Er^{3+}:YSO [58,59]. Due to the number of TE modes we see, we are not confident of the transverse mode numbers of the mode shown in Fig. 6(d), so we cannot predict its single-ion coupling constant. However, we can still calculate the transition dipole moment of $\mu_{\mathrm{TE}} = 3.7 \times 10^{-32}$ Cm and predict that the fundamental TE WGM will have a single-ion coupling rate of $2\pi \times 2.1$ kHz.

Figures 6(b) and 6(e) show the measured frequency shifts of these modes. At each magnetic-field value the microwave pump frequency ν_μ is slowly increased. Where the ground-state splitting of the erbium ions equals the microwave resonance frequency of 12.155 GHz the maximum shift is attained. The response is asymmetric, especially in Fig. 6(b), which is probably due to optical hole burning decreasing the response for frequencies above the Zeeman splitting. The phase response of these shifts is shown in Figs. 6(c) and 6(f) for measurements above the noise floor. The phase response of Fig. 6(c) further accentuates the asymmetry we attribute to optical hole burning for this optical frequency, which is closer to a bare erbium transition at these magnetic-field values. Note that the measurement in Figs. 6(e)–6(f) is performed when locked to the optical polariton at a field of about 75 mT. At this field the polariton is predominately photonlike; the polariton frequency is detuned from the bare erbium absorption frequency by about 2 GHz—five times larger than the expected optical linewidth of the erbium [60].

The EPR signal is due to the spin state coupling, which is proportional to $\sqrt{\Delta N} \propto (1 + P_\mu/P_s)^{-1/2}$, where $\Delta N = N_2 - N_1$ is the difference in population of the Zeeman levels and P_s is a saturation power. The saturation is assumed to be that of a simple driven two-level system. The fit to this is shown in Fig. 5, from which we find $P_s = -5.19(50)$ dBm.

The ODMR frequency shift of the optical mode saturates at high microwave power, as shown in Fig. 5. We fit this to an eye-guide fitting function to estimate the saturation of the signal:

$$\Delta\nu(P) = \Delta\nu_{\mathrm{max}}[1 - \exp(-P/P_{\mathrm{sat}})], \tag{3}$$

where $\Delta\nu_{\mathrm{max}}$ is the maximum attainable frequency shift and P_{sat} is the saturation microwave power. From this we find a saturation power of −0.54(15) dBm.

IV. DISCUSSION

We have shown that high Q factors can be obtained in cryogenic rare-earth-ion-doped whispering-gallery resonators, even when the modes are very close to optical transitions. The WGMs observed couple strongly to ensemble excitations of the 50 ppm erbium doping.

The modified ODMR spectroscopy we have described here is an elaboration of the technique to probe the spins with an optical resonance that is strongly coupled to an optical transition of the medium, i.e., the optical coupling rate to the

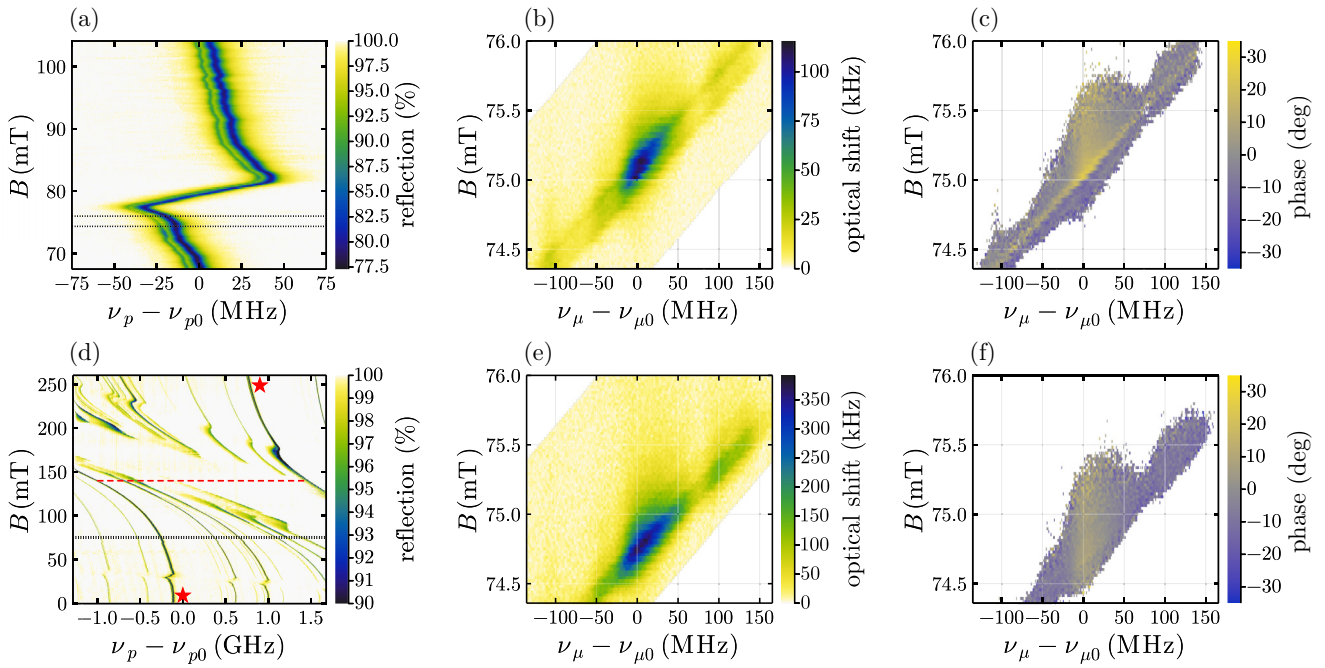

FIG. 6. (a) Frequency shift of a TE optical mode with magnetic field near a frequency of $\nu_{p0} = 195\,106.2(4)$ GHz. At a magnetic field of about 81 mT it crosses the $|2\rangle \leftrightarrow |3\rangle$ transition. (d) Frequency shift of a TE optical mode with magnetic field near a frequency of $\nu_{p0} = 195\,112.7(4)$ GHz. Between about 100 mT and 200 mT it avoids the $|2\rangle \leftrightarrow |4\rangle$ transition. Red stars at the top and bottom are located just beside the mode of interest and a red dashed line shows the mode splitting of 2.45 GHz. Black dotted lines in (a),(d) indicate the magnetic-field strengths examined in the other parts of this figure. (b),(e) Frequency shifts of the optical mode shown in (a),(d) when a magnetic field is applied along the D_2 axis and the microwave cavity is pumped at different frequencies. The diagonal line shows the Zeeman splitting of the Er^{3+}. Where this splitting equals the microwave resonance frequency of $\nu_{\mu 0} = 12.155$ GHz the maximum shift is attained. The magnetic-field values are converted directly from the currents set on the current sources. Hysteresis in the superconducting magnets causes an offset in current and hence an offset in assumed magnetic fields between the two measurements: (a)–(c) and (d)–(f). (c),(f) Relative phases of the response with respect to the modulating 1 kHz. The microwave input power into the cryostat for (b),(c),(e),(f) is 5 dBm, which is amplitude modulated at 1 kHz with a modulation depth of 45 %.

ensemble mode is much larger than the ensemble's optical linewidth. We have shown that we can measure the ODMR response with a polariton mode in the regime where it is mostly photonlike. The saturation microwave power for ODMR is similar to that of EPR [−0.54(15) dBm vs −5.19(50) dBm]. This shows that the microwave magnetic field is high in the optical mode volume, as the ODMR only probes the subclass of ions that live therein.

In the future we aim to observe Raman heterodyne [61] in the resonator for up-conversion. We have tried to observe Raman heterodyne in the system but could not. We believe this is due to the large imbalance in coupling rates for different erbium transitions[2] making the effective FSR significantly different from the microwave cavity frequency. The coupling rates between spin states can be made more even by careful choice of static magnetic-field direction [62,63]; such an orientation is not accessible in our current experimental configuration. Such Raman heterodyne is a stepping stone for coherent microwave-optical transduction, where adiabatic elimination of the excited states allows the process to have a high fidelity [19,21].

In conclusion, we report an erbium-doped WGM resonator sitting inside a microwave cavity for a modified ODMR measurement. The high Q-factor optical modes show strong coupling to ensemble erbium transitions. Our modified ODMR spectroscopy measures spin state through the changes in this coupling strength. We can therefore detect the spin transitions with an optical probe detuned by more than the inhomogeneous linewidth. Compared to EPR, strong-coupling ODMR has the capability of responding to only the ions within the optical-mode volume, which can be located in a region of a stronger average microwave field. Additionally, only those ions could be used for Raman heterodyne and therefore this characterization is important for future investigations to enable microwave-optical transduction.

[2]The coupling strength for transitions $|2\rangle \leftrightarrow |3\rangle$ and $|1\rangle \leftrightarrow |4\rangle$ is much weaker than $|2\rangle \leftrightarrow |4\rangle$ and $|1\rangle \leftrightarrow |3\rangle$; compare the splitting of the (anti)crossing in Figs. 6(a) and 6(d), as the coupling strength is half of the angular frequency splitting.

ACKNOWLEDGMENTS

This work was supported by the NZ Ministry of Business, Innovation and Employment (MBIE) Catalyst Strategic New Zealand–German Aerospace Centre Joint Research Programme Contract No. UOOX2112, and the USA Army Research Office (ARO/LPS) (CQTS) Grant No. W911NF1810011.

[1] P. Magnard, S. Storz, P. Kurpiers, J. Schär, F. Marxer, J. Lütolf, T. Walter, J.-C. Besse, M. Gabureac, K. Reuer, A. Akin, B. Royer, A. Blais, and A. Wallraff, Microwave Quantum Link between Superconducting Circuits Housed in Spatially Separated Cryogenic Systems, Phys. Rev. Lett. **125**, 260502 (2020).

[2] N. J. Lambert, A. Rueda, F. Sedlmeir, and H. G. L. Schwefel, Coherent conversion between microwave and optical photons—an overview of physical implementations, Adv. Quantum Technol. **3**, 1900077 (2020).

[3] N. Lauk, N. Sinclair, S. Barzanjeh, J. P. Covey, M. Saffman, M. Spiropulu, and C. Simon, Perspectives on quantum transduction, Quantum Sci. Technol. **5**, 020501 (2020).

[4] T. Böttger, C. W. Thiel, R. L. Cone, and Y. Sun, Effects of magnetic field orientation on optical decoherence in Er^{3+} : Y_2SiO_5, Phys. Rev. B **79**, 115104 (2009).

[5] Y. Sun, C. W. Thiel, R. L. Cone, R. W. Equall, and R. L. Hutcheson, Recent progress in developing new rare earth materials for hole burning and coherent transient applications, Proceedings of the Seventh International Meeting on Hole Burning, Single Molecules and Related Spectroscopies: Science and Applications, J. Lumin. **98**, 281 (2002).

[6] R. W. Equall, Y. Sun, R. L. Cone, and R. M. Macfarlane, Ultraslow Optical Dephasing in Eu^{3+} : Y_2SiO_5, Phys. Rev. Lett. **72**, 2179 (1994).

[7] R. L. Ahlefeldt, M. R. Hush, and M. J. Sellars, Ultranarrow Optical Inhomogeneous Linewidth in a Stoichiometric Rare-Earth Crystal, Phys. Rev. Lett. **117**, 250504 (2016).

[8] R. M. Macfarlane, A. Cassanho, and R. S. Meltzer, Inhomogeneous Broadening by Nuclear Spin Fields: A new Limit for Optical Transitions in Solids, Phys. Rev. Lett. **69**, 542 (1992).

[9] M. Zhong, M. P. Hedges, R. L. Ahlefeldt, J. G. Bartholomew, S. E. Beavan, S. M. Wittig, J. J. Longdell, and M. J. Sellars, Optically addressable nuclear spins in a solid with a six-hour coherence time, Nature (London) **517**, 177 (2015).

[10] A. Ortu, A. Tiranov, S. Welinski, F. Fröwis, N. Gisin, A. Ferrier, P. Goldner, and M. Afzelius, Simultaneous coherence enhancement of optical and microwave transitions in solid-state electronic spins, Nat. Mater. **17**, 671 (2018).

[11] J. V. Rakonjac, Y.-H. Chen, S. P. Horvath, and J. J. Longdell, Long spin coherence times in the ground state and in an optically excited state of Er^{3+} : Y_2SiO_5 at zero magnetic field, Phys. Rev. B **101**, 184430 (2020).

[12] M. C. Berrington, H. M. Rønnow, M. J. Sellars, and R. L. Ahlefeldt, Negative refractive index in dielectric crystals containing stoichiometric rare-earth ions, arXiv:2205.02739.

[13] D. Lago-Rivera, S. Grandi, J. V. Rakonjac, A. Seri, and H. de Riedmatten, Telecom-heralded entanglement between multimode solid-state quantum memories, Nature (London) **594**, 37 (2021).

[14] T. L. Harris, K. D. Merkel, R. K. Mohan, T. Chang, Z. Cole, A. Olson, and W. R. Babbitt, Multigigahertz range-Doppler correlative signal processing in optical memory crystals, Appl. Opt. **45**, 343 (2006).

[15] P. Berger, Y. Attal, M. Schwarz, S. Molin, A. Louchet-Chauvet, T. Chanelière, J.-L. L. Gouët, D. Dolfi, and L. Morvan, RF spectrum analyzer for pulsed signals: Ultra-wide instantaneous bandwidth, high sensitivity, and high time-resolution, J. Lightwave Technol. **34**, 4658 (2016).

[16] R. Kolesov, K. Xia, R. Reuter, R. Stöhr, A. Zappe, J. Meijer, P. R. Hemmer, and J. Wrachtrup, Optical detection of a single rare-earth ion in a crystal, Nat. Commun. **3**, 1029 (2012).

[17] J. M. Kindem, A. Ruskuc, J. G. Bartholomew, J. Rochman, Y. Q. Huan, and A. Faraon, Control and single-shot readout of an ion embedded in a nanophotonic cavity, Nature (London) **580**, 201 (2020).

[18] P. Jobez, I. Usmani, N. Timoney, C. Laplane, N. Gisin, and M. Afzelius, Cavity-enhanced storage in an optical spin-wave memory, New J. Phys. **16**, 083005 (2014).

[19] L. A. Williamson, Y.-H. Chen, and J. J. Longdell, Magneto-Optic Modulator with Unit Quantum Efficiency, Phys. Rev. Lett. **113**, 203601 (2014).

[20] E. Miyazono, T. Zhong, I. Craiciu, J. M. Kindem, and A. Faraon, Coupling of erbium dopants to yttrium orthosilicate photonic crystal cavities for on-chip optical quantum memories, Appl. Phys. Lett. **108**, 011111 (2016).

[21] X. Fernandez-Gonzalvo, S. P. Horvath, Y.-H. Chen, and J. J. Longdell, Cavity-enhanced raman heterodyne spectroscopy in Er^{3+} : Y_2SiO_5 for microwave to optical signal conversion, Phys. Rev. A **100**, 033807 (2019).

[22] D. Carbonera, Optically detected magnetic resonance (ODMR) of photoexcited triplet states, Photosynth. Res. **102**, 403 (2009).

[23] D. Suter, Optical detection of magnetic resonance, Magn. Reson. **1**, 115 (2020).

[24] B. M. Chernobrod and G. P. Berman, Spin microscope based on optically detected magnetic resonance, J. Appl. Phys. **97**, 014903 (2005).

[25] V. Jacques, P. Neumann, J. Beck, M. Markham, D. Twitchen, J. Meijer, F. Kaiser, G. Balasubramanian, F. Jelezko, and J. Wrachtrup, Dynamic Polarization of Single Nuclear Spins by Optical Pumping of Nitrogen-Vacancy Color Centers in Diamond at Room Temperature, Phys. Rev. Lett. **102**, 057403 (2009).

[26] P. Siyushev, K. Xia, R. Reuter, M. Jamali, N. Zhao, N. Yang, C. Duan, N. Kukharchyk, A. D. Wieck, R. Kolesov, and J. Wrachtrup, Coherent properties of single rare-earth spin qubits, Nat. Commun. **5**, 3895 (2014).

[27] D. V. Strekalov, C. Marquardt, A. B. Matsko, H. G. L. Schwefel, and G. Leuchs, Nonlinear and quantum optics with whispering gallery resonators, J. Opt. **18**, 123002 (2016).

[28] D. S. Norman, F. Azeem, J. J. Longdell, and H. G. L. Schwefel, Measuring optical loss in yttrium orthosilicate using a whis-

pering gallery mode resonator, Mater. Quantum. Technol. **2**, 011001 (2022).

[29] P. S. Kuo, J. Bravo-Abad, and G. S. Solomon, Second-harmonic generation using $\bar{4}$-quasi-phasematching in a GaAs whispering-gallery-mode microcavity, Nat. Commun. **5**, 3109 (2014).

[30] J. U. Fürst, K. Buse, I. Breunig, P. Becker, J. Liebertz, and L. Bohatý, Second-harmonic generation of light at 245 nm in a lithium tetraborate whispering gallery resonator, Opt. Lett. **40**, 1932 (2015).

[31] L. S. Trainor, F. Sedlmeir, C. Peuntinger, and H. G. L. Schwefel, Selective Coupling Enhances Harmonic Generation of Whispering-Gallery Modes, Phys. Rev. Appl. **9**, 024007 (2018).

[32] T. Herr, V. Brasch, J. D. Jost, C. Y. Wang, N. M. Kondratiev, M. L. Gorodetsky, and T. J. Kippenberg, Temporal solitons in optical microresonators, Nat. Photon. **8**, 145 (2014).

[33] K. E. Webb, M. Erkintalo, S. Coen, and S. G. Murdoch, Experimental observation of coherent cavity soliton frequency combs in silica microspheres, Opt. Lett. **41**, 4613 (2016).

[34] S.-K. Meisenheimer, J. U. Fürst, K. Buse, and I. Breunig, Continuous-wave optical parametric oscillation tunable up to an 8 μm wavelength, Optica **4**, 189 (2017).

[35] M. Förtsch, G. Schunk, J. U. Fürst, D. Strekalov, T. Gerrits, M. J. Stevens, F. Sedlmeir, H. G. L. Schwefel, S. W. Nam, G. Leuchs, and C. Marquardt, Highly efficient generation of single-mode photon pairs from a crystalline whispering-gallery-mode resonator source, Phys. Rev. A **91**, 023812 (2015).

[36] J. U. Fürst, D. V. Strekalov, D. Elser, A. Aiello, U. L. Andersen, Ch. Marquardt, and G. Leuchs, Quantum Light from a Whispering-Gallery-Mode Disk Resonator, Phys. Rev. Lett. **106**, 113901 (2011).

[37] A. A. Savchenkov, W. Liang, A. B. Matsko, V. S. Ilchenko, D. Seidel, and L. Maleki, Tunable optical single-sideband modulator with complete sideband suppression, Opt. Lett. **34**, 1300 (2009).

[38] M. Zhang, B. Buscaino, C. Wang, A. Shams-Ansari, C. Reimer, R. Zhu, J. M. Kahn, and M. Lončar, Broadband electro-optic frequency comb generation in a lithium niobate microring resonator, Nature (London) **568**, 373 (2019).

[39] A. Rueda, F. Sedlmeir, M. Kumari, G. Leuchs, and H. G. L. Schwefel, Resonant electro-optic frequency comb, Nature (London) **568**, 378 (2019).

[40] J. A. Haigh, N. J. Lambert, S. Sharma, Y. M. Blanter, G. E. W. Bauer, and A. J. Ramsay, Selection rules for cavity-enhanced Brillouin light scattering from magnetostatic modes, Phys. Rev. B **97**, 214423 (2018).

[41] S. J. Herr, K. Buse, and I. Breunig, LED-pumped whispering-gallery laser, Photon. Res. **5**, B34 (2017).

[42] N. Toropov, G. Cabello, M. P. Serrano, R. R. Gutha, M. Rafti, and F. Vollmer, Review of biosensing with whispering-gallery mode lasers, Light Sci. Appl. **10**, 42 (2021).

[43] F. Azeem, L. S. Trainor, A. Gao, M. Isarov, D. V. Strekalov, and H. G. L. Schwefel, Ultra-low threshold titanium-doped sapphire whispering-gallery laser, Adv. Opt. Mater. **10**, 2102137 (2022).

[44] D. L. McAuslan, D. Korystov, and J. J. Longdell, Coherent spectroscopy of rare-earth-metal-ion-doped whispering-gallery-mode resonators, Phys. Rev. A **83**, 063847 (2011).

[45] I. S. Grudinin, V. S. Ilchenko, and L. Maleki, Ultrahigh optical Q factors of crystalline resonators in the linear regime, Phys. Rev. A **74**, 063806 (2006).

[46] Y. Sun, T. Böttger, C. W. Thiel, and R. L. Cone, Magnetic g tensors for the $^4I_{15/2}$ and $^4I_{13/2}$ states of Er^{3+} : Y_2SiO_5, Phys. Rev. B **77**, 085124 (2008).

[47] A. Rueda, F. Sedlmeir, M. C. Collodo, U. Vogl, B. Stiller, G. Schunk, D. V. Strekalov, C. Marquardt, J. M. Fink, O. Painter, G. Leuchs, and H. G. L. Schwefel, Efficient microwave to optical photon conversion: An electro-optical realization, Optica **3**, 597 (2016).

[48] M. Mitsunaga, E. S. Kintzer, and R. G. Brewer, Raman heterodyne interference: Observations and analytic theory, Phys. Rev. B **31**, 6947 (1985).

[49] E. S. Kintzer, M. Mitsunaga, and R. G. Brewer, Raman heterodyne interference: Symmetry analysis, Phys. Rev. B **31**, 6958 (1985).

[50] H. Hirata, T. Kuyama, M. Ono, and Y. Shimoyama, Detection of electron paramagnetic resonance absorption using frequency modulation, J. Magn. Reson. **164**, 233 (2003).

[51] J. S. Hyde, W. Froncisz, J. W. Sidabras, T. G. Camenisch, J. R. Anderson, and R. A. Strangeway, Microwave frequency modulation in CW EPR at W-band using a loop-gap resonator, J. Magn. Reson. **185**, 259 (2007).

[52] Y.-H. Chen, X. Fernandez-Gonzalvo, S. P. Horvath, J. V. Rakonjac, and J. J. Longdell, Hyperfine interactions of Er^{3+} ions in Y_2SiO_5: Electron paramagnetic resonance in a tunable microwave cavity, Phys. Rev. B **97**, 024419 (2018).

[53] L. Neuhaus, R. Metzdorff, S. Chua, T. Jacqmin, T. Briant, A. Heidmann, P.-F. Cohadon, and S. Deléglise, PyRPL (Python Red Pitaya Lockbox) - an open-source software package for FPGA-controlled quantum optics experiments, in *2017 European Conference on Lasers and Electro-Optics and European Quantum Electronics Conference* (IEEE, New York, 2017), p. EA_P_8.

[54] C. Yu, J. Janousek, E. Sheridan, D. L. McAuslan, H. Rubinsztein-Dunlop, P. K. Lam, Y. Zhang, and W. P. Bowen, Optomechanical Magnetometry with a Macroscopic Resonator, Phys. Rev. Appl. **5**, 044007 (2016).

[55] J. Li, H. Lee, K. Y. Yang, and K. J. Vahala, Sideband spectroscopy and dispersion measurement in microcavities, Opt. Express **20**, 26337 (2012).

[56] Y. A. Demchenko and M. L. Gorodetsky, Analytical estimates of eigenfrequencies, dispersion, and field distribution in whispering gallery resonators, J. Opt. Soc. Am. B **30**, 3056 (2013).

[57] I. Breunig, B. Sturman, F. Sedlmeir, H. G. L. Schwefel, and K. Buse, Whispering gallery modes at the rim of an axisymmetric optical resonator: Analytical versus numerical description and comparison with experiment, Opt. Express **21**, 30683 (2013).

[58] D. L. McAuslan, J. J. Longdell, and M. J. Sellars, Strong-coupling cavity QED using rare-earth-metal-ion dopants in monolithic resonators: What you can do with a weak oscillator, Phys. Rev. A **80**, 062307 (2009).

[59] C. W. Thiel, T. Böttger, and R. L. Cone, Rare-earth-doped materials for applications in quantum information storage and signal processing, Selected Papers from DPC'10, J. Lumin. **131**, 353 (2011).

[60] T. Böttger, Y. Sun, C. W. Thiel, and R. L. Cone, Spectroscopy and dynamics of $Er^{3+} : Y_2SiO_5$ at 1.5 μm, Phys. Rev. B **74**, 075107 (2006).

[61] J. Mlynek, N. C. Wong, R. G. DeVoe, E. S. Kintzer, and R. G. Brewer, Raman Heterodyne Detection of Nuclear Magnetic Resonance, Phys. Rev. Lett. **50**, 993 (1983).

[62] X. Fernandez-Gonzalvo, Y.-H. Chen, C. Yin, S. Rogge, and J. J. Longdell, Coherent frequency up-conversion of microwaves to the optical telecommunications band in an Er:YSO crystal, Phys. Rev. A **92**, 062313 (2015).

[63] G. G. G. King, P. S. Barnett, J. G. Bartholomew, A. Faraon, and J. J. Longdell, Probing strong coupling between a microwave cavity and a spin ensemble with Raman heterodyne spectroscopy, Phys. Rev. B **103**, 214305 (2021).